Vol 13 No 6, June 2004
1009-1963/2004/13(06)/0871-06

Chinese Physics

© 2004 Chin. Phys. Soc.
and IOP Publishing Ltd

Theoretical and experimental investigations of quasi-continuous wave diode array side-pumped Yb:YAG slab laser

Wu Hai-Sheng(吴海生)†, Yan Ping(闫 平),
Gong Ma-Li(巩马理), and Liu Qiang(柳 强)

Department of Precision Instruments, Tsinghua University, Beijing 100084, *China*

(Received 24 September 2003; revised manuscript received 5 February 2004)

An analytical model of quasi-continuous wave (quasi-CW) diode array side-pumped slab laser for Yb:YAG oscillator in long-pulse free-running has been developed based on the CW model. In this model we first introduce a new parameter, pump pulse width, and make the model available for use in the quasi-CW model. We also give an analytical equation of laser delay time to calculate the laser pulse width. A detailed model is also presented for a new structure laser design, taking account of the geometry of Yb:YAG slab. A quasi-CW diode array side-pumped Yb:YAG slab laser is investigated theoretically and experimentally. Experiments yield a quasi-CW output energy up to 20.36 mJ with the laser pulse width of 654.55 μs at 1049 nm when the diode arrays operate at 25 Hz and 1 ms pulse width. The crystal dimensions are 3 mm×8 mm×1 mm and the doping density is 10 at.%. The experimental results are in good agreement with the predictions of the theoretical model.

Keywords: quasi-continuous wave diode array side-pumped, Yb:YAG, laser delay time, pump pulse width, lensduct

PACC: 4255R, 4260D

1. Introduction

With the development of high brightness laser diodes, quasi-three-level lasers have been investigated in recent years, in which Yb-doped laser crystals offer the spectroscopic and laser properties that make them a promising candidate for high-power 1 μm laser systems.[1−14] Particularly, the Yb:YAG crystal has a long storage lifetime of 951 μs [15] and a very low quantum defect (8.6%). Thus the Yb:YAG laser generates less heat than the Nd:YAG laser under the same output power condition. In addition, the pump transition at 941 nm makes this material highly suitable for diode pumping, using InGaAs diodes which are potentially more robust than the AlGaAs diodes used to excite Nd:YAG at 808 nm. Another advantage of the Yb:YAG laser is that the 941 nm absorption feature is approximately five times broader than the Nd:YAG's 808 nm absorption feature, therefore the Yb:YAG system is less sensitive to diode wavelength specifications.

Yb:YAG lasers have been demonstrated in a variety of configurations such as microchip,[1−3] waveguides,[4,5] end-pumped rod [6] and side-pumped rod,[7] thin disc geometries [8] and end-pumped slab [9] side-pumped slab,[10−12] and zig-zag edge-pumped slab.[13] Several theoretical investigations [16−20] are proposed to optimize the different configurations of quasi-three-level continuous wave (CW) lasers. However, these models of CW laser without including the pump pulse width are hard to apply to a quasi-CW side-pumped slab laser directly. Although Ter-Mikirtychev *et al*[21] develop an end-pumped model of quasi-CW laser, it is also difficult to apply to the side-pumped slab structure. The laser delay time is also an important quantity in quasi-CW lasers system, for it determines the laser pulse width and affects the solution of the problem of pulse synchronization design. Although Ter-Mikirtychev *et al*'s model gave an analytic solution to the equation of the laser delay time, the equation has not been demonstrated to be valid in related experiments.

In this paper, we develop a quasi-CW model by improving the CW model of side-pumped Yb:YAG

†E-mail: wuhs99@mails.tsinghua.edu.cn

laser oscillator, following Beach's approach [17] and Rutherford *et al*'s method.[19] The pump pulse width is firstly introduced in the model that can be used to design the quasi-CW side-pumped slab laser. An analytic equation of laser delay time is also presented and demonstrated by experiments. A novel structure of side-pumped Yb:YAG slab laser is set up. The diode arrays is not pre-collimated by microlens, and the pump light is directly coupled into Yb:YAG crystal by a lensduct. In Section 2 we define the new side-pumped structure shown in Fig.1 and derive the pump absorption coefficient. In Section 3, we give a set of equations to include an analytic relationship between the input pump and output laser energy, taking the pump pulse width into account. The analytic equation of the laser delay time is also given, which is different from that reported in Ref.[21]. At the end of Section 4, the experimental and theoretical results are analysed. The output energy of 20.36 mJ with the laser pulse width of 654.55 μs at 1049 nm has been obtained.

2. Definition of side-pumped structure

The side-pumped geometry is shown in Fig.1. In the side-pumped slab, the pump light is incident normal into the crystal. Through single-pass absorption the unabsorbed pump light is reflected back by another face coated with HR@941 nm for a second pass through the crystal, which is also the cooling plane. The thickness of the crystal can be larger than the pump thickness T in order to enlarge the radiating area for efficient cooling. With this geometry, the main challenge is to achieve uniform pump absorption along the width. We assume the pump beam light to be uniform plane waves for simplicity. In reality, the pump light has some divergence and intensity nonuniformities.

We define a coordinate system for the slab. The x direction is along the thickness, y is along the width, and z is along the length. The full thickness is T, the full width is w, the full pump thickness is W ($W < w$), and the full length is L.

The side-pumped design has a benefit: excellent thermal management. The heat load of the quasi-CW diode array pumped system is far less than that of the CW diode array pumped system. The larger cooling face for the side-pumped structure can realize an efficient cooling (the crystal width $w \gg W$); the thin crystal is of advantage to the thermal conduction due to the high doping density. However, the high doping can lead to amplified spontaneous emission (ASE) and low stored energy, thus lower doping must be adopted in order to prevent ASE in a high output energy system.

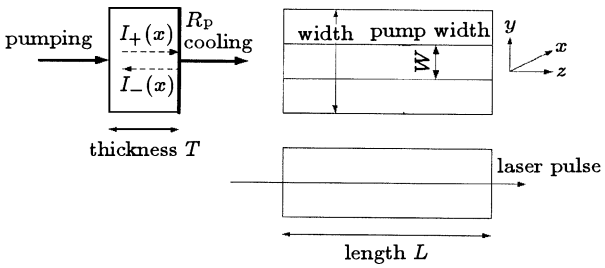


Fig.1. Orthographic drawing of a side-pumped slab.

In this slab, $I_+(x)$ and $I_-(x)$ are the pump intensities along the x and $-x$ directions respectively. In this case, the pump light is absorbed in a double-pass through the slab. The absorbed peak power intensity (similar to that in Ref.[19]) as a function of the position x along the slab width is given by

$$\begin{aligned}\rho_{\rm abs}(x) =& -\frac{{\rm d}I_+(x)}{{\rm d}x} + \frac{{\rm d}I_-(x)}{{\rm d}x} \\ =& \frac{\alpha P}{WL}\exp\left(-\alpha\left(x+\frac{T}{2}\right)\right) \\ &+ \frac{\alpha R_{\rm p} P}{WL}\exp\left(\alpha\left(x-\frac{3T}{2}\right)\right), \end{aligned} \quad (1)$$

where P is the total pump peak power incident on the slab, α the pump absorption coefficient, and $R_{\rm p}$ ($R_{\rm p} > 99.5\%$) the reflectivity of the cooling face at pump light of 941 nm.

Using Eq.(1), the pumping absorption efficient $\eta_{\rm abs}$ is expressed as

$$\begin{aligned}\eta_{\rm abs} =& \frac{WL\int_{-T/2}^{+T/2}\rho_{\rm abs}(x){\rm d}x}{P} \\ =& 1 - R_{\rm p}\exp(-2\alpha T) + \exp(-\alpha T)(R_{\rm p}-1), \end{aligned} \quad (2)$$

$\eta_{\rm abs} \approx 1 - \exp(-2\alpha T)$ for $R_{\rm p} \approx 1$.

3. Modelling of side-pumped quasi-CW lasers

The energy level diagram of Yb:YAG is shown in Fig.2. There are only two manifolds: three energy levels in upper manifold $^2F_{5/2}$ and four energy levels in lower manifold $^2F_{7/2}$. This quasi-three-level structure results in the absence of intermediate and high-lying energy manifolds. Therefore,

no concentration quenching, no excited-state absorption and no up-conversion appear in the Yb:YAG medium. The 18 nm infrared absorption linewidth at 941 nm is ideal for InGaAs diode pumping. The wide enough linewidth reduces the difficulty of controlling pump wavelength. The emission bands of Yb:YAG have two peaks at 1030 and 1049 nm. In our previous works, the laser wavelength measured is 1049 nm.[2,10] But the emission cross section at 1030 nm (3.3×10^{-20} cm^2) is greater than that at 1049 nm by about 0.3×10^{-20} cm^2,[21] and the output energy will be influenced greatly. The long excited-state lifetime of 951 μs leads to the excellent energy storage of the Yb:YAG. The smaller wavelength difference between pump and laser results in few quantum defects and low heat load.

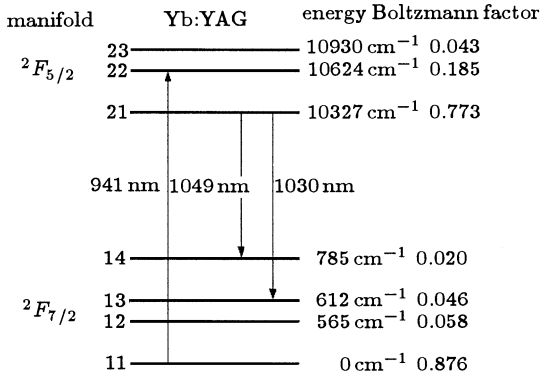


Fig.2. Energy level diagram of Yb:YAG.

The population densities satisfy

$$n_{\rm d} = n_{\rm L} + n_{\rm U}, \tag{3}$$

$$n_{1i} = f_{1i} \times n_{\rm L}, \quad n_{2j} = f_{2j} \times n_{\rm U}, \tag{4}$$

where $n_{\rm d}$ is the total doping population density, $n_{\rm U}$ and $n_{\rm L}$ are the population densities of upper and lower energy levels respectively; f_{1i} and f_{2j} are the Boltzmann occupation factors of the Stark levels i and j of the lower and upper levels, respectively. Using this notation, the rate equation for the upper level may be expressed as

$$\frac{{\rm d}n_{\rm U}}{{\rm d}t} = \eta_{\rm abs}\frac{\eta_{\rm trans}P}{h\nu_{\rm p}WTL} - c\sigma_{\rm l}\Delta n\phi - \frac{n_{\rm U}}{\tau}, \tag{5}$$

where $\eta_{\rm trans}$ is the pump transmission efficiency between the diode arrays and the Yb:YAG crystal; $h\nu_{\rm p}$ is the pump photo energy, Δn the inversion population density, ϕ the laser photo density, $\sigma_{\rm l}$ the emission cross section, c the velocity of light, and τ the excited-state lifetime.

We first assume that the laser mode completely fills the pump area of the slab and that the pump distribution is uniform. Our quasi-CW model is based on Beach's approach [17] and Rutherford *et al*'s approach.[19] In this model, we introduce a new parameter for free-running operation: the pump pulse width $t_{\rm p}$. The overall excitation population from the lower manifold to the upper manifold is then

$$N_{\rm lower\to upper} = \eta_{\rm abs}\frac{\eta_{\rm trans}Pt_{\rm p}}{h\nu_{\rm p}}, \tag{6}$$

and the overall de-excitation population (including the stimulated emission and spontaneous emission) can be written as

$$\begin{aligned} N_{\rm upper\to lower} =& \frac{E_{\rm out}}{h\nu_{\rm l}}\frac{R_{\rm oc}}{1-R_{\rm oc}}\{[\exp(\sigma_{\rm l}\Delta nL)-1] \\ &+ (1-\delta)^2[\exp(2\sigma_{\rm l}\Delta nL) \\ &- \exp(\sigma_{\rm l}\Delta nL)]\} + \frac{n_{\rm U}WTLt_{\rm p}}{\tau}, \end{aligned} \tag{7}$$

where $E_{\rm out}$ is the laser output energy, $h\nu_{\rm l}$ the laser photo energy, $R_{\rm oc}$ the output mirror reflectivity, and δ the one-way cavity loss.

After the inversion population reaches the threshold, it becomes zero. The round-trip gain is equal to unity. Solving equations $(1-\delta)^2R_{\rm oc}\exp(2\sigma_{\rm l}\Delta nL) = 1$, $\Delta n = f_{21}n_{\rm U} - f_{1i}n_{\rm L}$ and Eq.(3), the upper manifold population density $n_{\rm U}$ is found:[19]

$$\begin{aligned} n_{\rm U} =& \frac{f_{1i}}{f_{21}+f_{1i}}n_{\rm d} + \frac{1}{2(f_{21}+f_{1i})\sigma_{\rm l}L} \\ &\times \ln\left[\frac{1}{(1-\delta)^2R_{\rm oc}}\right]. \end{aligned} \tag{8}$$

In Eq.(2), α is rewritten as [19]

$$\begin{aligned} \alpha =& \sigma_{\rm p}(f_{11}n_{\rm L} - f_{22}n_{\rm U}) \\ =& \sigma_{\rm p}\left[\frac{f_{11}(f_{21}+f_{1i}) - f_{1i}(f_{11}+f_{22})}{f_{21}+f_{1i}}n_{\rm d}\right. \\ &\left. - \frac{f_{11}+f_{22}}{f_{21}+f_{1i}}\frac{1}{2\sigma_{\rm l}L}\ln\left(\frac{1}{(1-\delta)^2R_{\rm oc}}\right)\right], \end{aligned} \tag{9}$$

where $\sigma_{\rm p}$ is the absorption cross section. At a steady state, the excitation population (6) must be equal to the de-excitation population (7). Solving $N_{\rm lower\to upper} = N_{\rm upper\to lower}$ by using Eq.(8), then $E_{\rm out}$ is given by

$$\begin{aligned} E_{\rm out} =& \frac{\nu_{\rm l}}{\nu_{\rm p}}\frac{1-R_{\rm oc}}{1-R_{\rm oc}+\sqrt{R_{\rm oc}}\left(\dfrac{1}{1-\delta}+\delta-1\right)} \\ &\times\left(\eta_{\rm abs}E_{\rm in} - \frac{h\nu_{\rm p}f_{1i}n_{\rm d}WTLt_{\rm p}}{(f_{21}+f_{1i})\tau}\right. \\ &\left. - \frac{h\nu_{\rm p}WTt_{\rm p}}{2(f_{21}+f_{1i})\sigma_{\rm l}\tau}\ln\left[\frac{1}{(1-\delta)^2R_{\rm oc}}\right]\right), \end{aligned} \tag{10}$$

where $E_{\rm in} = Pt_{\rm p}$.

In quasi-CW laser oscillators, the time from the beginning of the pump pulse to the beginning of the laser pulse is defined as a laser delay time $t_{\rm delay}$. It can be solved from the following differential equation when the laser photo density ϕ=0 and $n_{\rm U} = n_{\rm Uth}$:

$$\frac{{\rm d}n_{\rm U}}{{\rm d}t} = \eta_{\rm abs}\frac{\eta_{\rm trans}P}{h\nu_{\rm p}WTL} - \frac{n_{\rm U}}{\tau}, \qquad (11)$$

where $n_{\rm Uth}$ is given by Eq.(8). But $\eta_{\rm abs}(n_{\rm U})$ is an implicit equation. Equation (11) must be solved by numerical solution. At the beginning of pump, $n_{\rm L} \approx n_{\rm d}$ and $\eta_{\rm abs} \approx 1 - \exp(-2\sigma_{\rm p} f_{11} n_{\rm L} W)$. As the pump peak power grows, the limiting normalized population density difference between the two manifolds approaches the following value:[18]

$$\frac{n_{\rm U} - n_{\rm L}}{n_{\rm d}} \to \frac{f_{11} - f_{22}}{f_{11} + f_{22}} = 0.64938. \qquad (12)$$

The minimum $n_{\rm L}$ can be given from the two equations (12) and (3) and $n_{\rm L}^{\rm min} = 0.825 n_{\rm d}$, then $n_{\rm L}$ can be verified from $n_{\rm d}$ to $0.825 n_{\rm d}$ with increasing pump peak power. Therefore, we assume that $\eta_{\rm abs}$ is a constant and $n_{\rm L} \approx n_{\rm d}$ because $n_{\rm L}^{\rm min}$ cannot be reached even for strong pumping, and then Eq.(11) can be solved analytically:

$$t_{\rm delay} = \tau\left[\ln\left(\frac{\eta_{\rm abs}\eta_{\rm trans}P}{h\nu_{\rm p}WTL}\right) - \ln\left(\frac{\eta_{\rm abs}\eta_{\rm trans}P}{h\nu_{\rm p}WTL} - \frac{n_{\rm Uth}}{\tau}\right)\right]. \qquad (13)$$

4. Theoretical and experimental results

Figure 3 shows the schematic of the diode-arrays side-pumped Yb:YAG laser oscillator. The laser crystal is a slab-shaped 10% doped, 3 mm×8 mm×1 mm Yb:YAG, which has an AR coating on two 8 mm×1 mm flat face, an AR coating on the 3 mm×8 mm pump surface and a HR coating on the cooling face. It is mounted in a copper sink and water cooled down to 10°C. In order to cool the Yb:YAG efficiently an indium foil is inserted between the laser crystal and the copper sink. The Yb:YAG crystal is pumped by the microlens-free 8-bar, 0.8 mm pitch, InGaAs diode arrays (Hi-Tech Optoelectronics Co., Ltd.) with an emitting area of $10\times5.6\,{\rm mm}^2$. The divergence angles of the diode arrays are 10° and 40° (FWHM) in slow axis and fast axis, respectively. Each bar can produce peak power of as much as 47 W, and the maximum output energy is about 375 mJ when the diode arrays are operated at a repetition rate of 25 Hz and a pulse width of 1 ms using LDI-928-25 (Laser Drive, Inc.) and done with a cooling water temperature of 11.8°C to yield the desired pump wavelength of 941 nm. By the lensduct the pump light is concentrated into the Yb:YAG slab crystal through total internal reflection. A plano-concave cavity, which has a length about 25 cm, is composed of a concave output mirror and a plane front mirror, whose reflectivity is greater than 99.9%. In this experiment, the laser beam propagated straight (not zig-zag) inside the slab crystal.

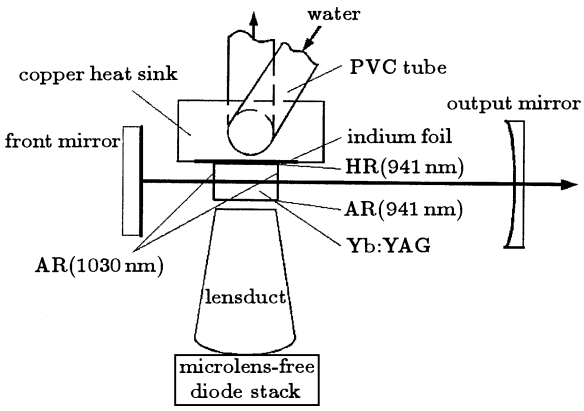


Fig.3. Schematic diagram of a quasi-CW diode-array side-pumped Yb:YAG oscillator.

As a coupler, the 51 mm-length lensduct, whose compression ratios in slow axis and fast axis are 8.75:1 and 2.42:1 respectively, is used to condense the pump light and smooth the profile of the diode pump light. Its input face is a spherical face and the output face is a plane. After exiting the lensduct, the pump light is condensed down to 1.2 mm×2.8 mm and focused on a pump spot of 1.3 mm×2.9 mm on the pump surface (AR@941 nm) of the Yb:YAG crystal. Figure 4 shows the transmission efficiency of the lensduct as a function of its length and the intensity profile of the diode pump light on the area (1.4 mm×3 mm) of the crystal pump surface. Using the Zemax software, the transmission efficiency of 82.7% is predicted without AR coating on the input and output surfaces in theory, whereas the measured efficiency is about 80%. The two results agree well.

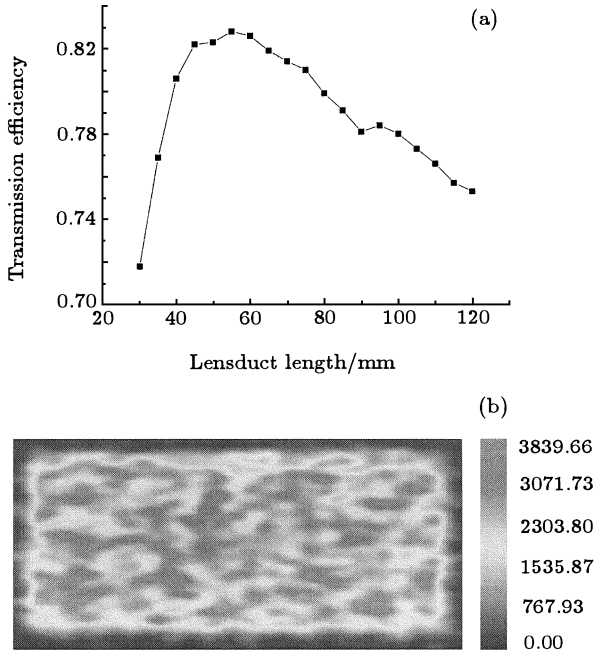


Fig.4. The transmission efficiency of the lensduct as a function of its length (a). The intensity profile of the diode pump light on the area of 3 mm×1.4 mm of the crystal's pump surface (b).

In this experiment, a model 1554 photo detector (12 GHz, New Focus Inc.) and a 54845A oscilloscope (1.8 GHz, 8 G/s sampling rate, Agilent Inc.) are used to receive and display the pulse. The output energy and beam quality of the Yb:YAG laser are measured by an EPM2000 energy meter (Molectron Detector Inc.) and M^2-200 beam propagation analyser (Spiricon Inc.), respectively. We also measure the laser wavelength using a 86142B spectrum analyser (Agilent Inc.).

We do not obtain the 1030 nm laser output as expected, but achieve a 1049.3 nm laser output. The reason is that the absorption at the wavelength of 1030 nm is higher than the gain at the same wavelength. The beam quality factor M^2 values are 5.93 and 8.01 in the vertical and horizontal directions respectively. The beam waists in the two directions are 0.5642 and 0.6408 mm.

Taking into account the mode match efficiency ($\eta_{\rm mode} = 0.6$) in Eqs.(9)–(11) and the mode volume (because the laser mode cannot completely fill the pump area of the slab in fact, here W, T and L are considered as the width, the thickness and the length of the mode volume respectively. W=0.6 mm, T=0.6 mm, L=3 mm), the theoretical results (continuous line) and experimental results (asterisks) of the output energy are shown in Fig.5. The output energy of 20.36 mJ is measured at 70 A, and the pump energy threshold is about 172 mJ. Figure 6 shows the laser pulse width ($t_{\rm p} - t_{\rm delay}$) versus the pump energy for the measured, numerical and analytic results. The numerical results are in better agreement with the measured results than the analytic results at a higher pump energy, but the analytic solutions also can give a good estimate for laser pulse width ($t_{\rm p} - t_{\rm delay}$) at a lower pump energy. This phenomenon results from the hypothesis of $n_{\rm L} \approx n_{\rm d}$. The laser pulse width of 654.55 μs, which is shown in Fig.7 with the pump pulse of the diode arrays, is obtained at 70 A. All the experimental results show a good agreement with the theoretical results.

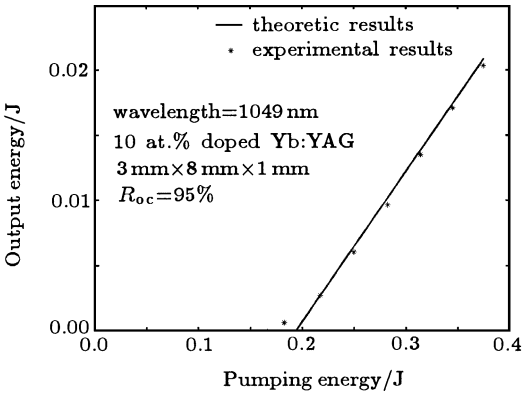


Fig.5. Experimental (asterisk) and theoretical (continuous lines) results for the dependences of the output energy on the pump energy.

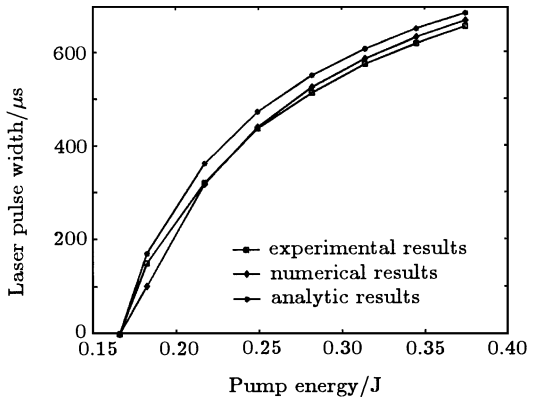


Fig.6. The laser pulse width versus the pump energy.

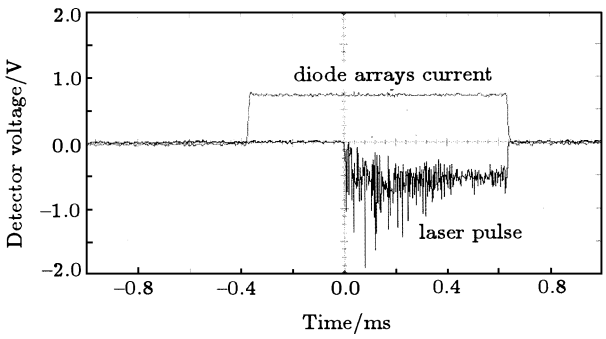


Fig.7. Typical measured results of Yb:YAG laser pulse and 1 ms pump pulse.

5. Conclusion

A model for quasi-CW diode-array side-pumped quasi-three-level Yb:YAG slab oscillator has been developed, and can be applied to the quasi-CW slab laser system design. We give a set of analytic expressions for the relation between the pump energy and the output energy including the pump pulse width. The analytic equation of laser delay time is also given, which can provide an estimate of laser pump width and a reference as the sequential control of laser pulse. The feature is also demonstrated for the quasi-CW microlens-free diode-array side-pumped Yb:YAG laser. The device uses the lensduct as a coupling element that can increase the coupling efficiency of the microlens-free diode arrays and improve the pump uniformity. Around 5.4% optical-to-optical efficiency and 20.36 mJ laser output energy with laser pulse width of 654.55 μs at 1049 nm are achieved using a 3 mm×8 mm×1 mm(10 at.%) Yb:YAG crystal when the quasi-CW microlens-free diode arrays are operated at a repetition rate of 25 Hz and the pump pulse width of 1 ms. The experimental results verify that the theoretical model is valid for designing the quasi-three-level laser system of the quasi-CW free-running operation.

References

[1] Lacovara P, Choi H L, Wang C A *et al* 1991 *Opt. Lett.* **16** 1089

[2] Wu H S, Yan P, Gong M L *et al* 2002 *Chin. J. Lasers* **11** 961 (in Chinese)

[3] Fan T, Klunk S and Henein G 1993 *Opt. Lett.* **18** 423

[4] Pelenc D, Large A C and Tropper A C 1995 *Opt. Commun.* **115** 491

[5] Griebner U, Grunwald R and Schonnagel F 1999 *Opt. Commun.* **164** 185

[6] Beach R J, Honea E C, Sutton S B *et al* 2000 *Proc. SPIE* **3889** 246

[7] Sumida D S, Bruesselbach H and Byren R W 1998 *Proc. SPIE* **3265** 100

[8] Giesen A, Hugel H, Voss A *et al* 1994 *Appl. Phys. B: Photophys. Laser Chem.* **58** 365

[9] Mandl A and Klimek P E 2001 *Proc. SPIE* **4267** 1

[10] Wu H S, Yan P, Gong M L *et al* 2002 *Proc. SPIE.* **4914** 14

[11] Sato M, Iehisa N and Karube N 2000 *Proc. SPIE* **3889** 208

[12] Sumida D S and Fan T Y 1995 *Opt. Lett.* **20** 2384

[13] Rutherford T S, Tukkoch W M, Sinha S *et al* 2001 *Opt. Lett.* **26** 986

[14] Yang H, Zhao Z W, Zhang J *et al* 2001 *Chin. Phys.* **10** 1136

[15] Sumida D S and Fan T Y 1994 *Opt. Lett.* **19** 1343

[16] Taira T, Tulloch W M and Byer R L 1997 *Appl. Opt.* **36** 1867

[17] Beach R J 1996 *Opt. Commun.* **123** 385

[18] Lim C and Izawa Y 2002 *IEEE J. Quant. Electron.* **38** 306

[19] Rutherford T S, Tulloch W M, Gustafson E K *et al* 2000 *IEEE J. Quant. Electron.* **36** 205

[20] Contag K, Karszewski M, Stewen C *et al* 1999 *Quant. Electron.* **29** 687

[21] Ter-Mikirtychev V V, Dubinskii M A and Fromzel V A 2001 *Opt. Commun.* **197** 403